Accepted version

Please cite as: Gori, S., Falcucci, E., Galadini, F., Zimmaro, P., Pizzi, A., Kayen, R. E., ... & Stewart, J. P. (2018). "Surface faulting caused by the 2016 central Italy seismic sequence: Field mapping and LiDAR/UAV imaging". Earthquake Spectra, 34(4), 1585-1610, DOI:10.1193/111417EQS236MR

Surface Faulting Caused by the 2016 Central Italy Seismic Sequence: Field Mapping and LiDAR/UAV Imaging

Stefano Gori,[a] Emanuela Falcucci,[a] Fabrizio Galadini,[a] Paolo Zimmaro,[b] M.EERI, Alberto Pizzi,[c] Robert E. Kayen,[d] M.EERI, Bret N. Lingwall,[e] M.EERI, Marco Moro,[a] Michele Saroli,[a] Giandomenico Fubelli,[f] Alessandra Di Domenica,[c] and Jonathan P. Stewart,[b] M.EERI

ABSTRACT

The three The three mainshock events (M6.1 24 August, M5.9 26 October, and M6.5

30 October 2016) in the Central Italy earthquake sequence produced surface rup- tures on known segments of the Mt. Vettore–Mt. Bove normal fault system. As a result, teams from Italian national research institutions and universities, working collaboratively with the U.S. Geotechnical Extreme Events Reconnaissance Association (GEER), were mobilized to collect perishable data. Our reconnais- sance approach included field mapping and advanced imaging techniques, both directed towards documenting the location and extent of surface rupture on the main fault exposure and secondary features. Mapping activity occurred after each mainshock (with different levels of detail at different times), which provides data on the progression of locations and amounts of slip between events. Along the full length of the Mt. Vettore–Mt. Bove fault system, vertical offsets ranged from 0–35 cm and 70–200 cm for the 24 August and 30 October events, respectively. Comparisons between observed surface rupture displacements and available empirical models show that the three events fit within expected ranges.

a) Istituto Nazionale di Geofisica e Vulcanologia (INGV), Italy
b) Department of Civil and Environmental Engineering, University of California Los Angeles, Los Angeles, CA
c) Dipartimento di Ingegneria e Geologia, Università degli Studi di Chieti-Pescara, Italy
d) United States Geological Survey (USGS), Berkeley, CA
e) Department of Civil and Environmental Engineering, South Dakota School of Mines & Technology, Rapid City, SD; Email: blingwall@kleinfelder.com (BNL, corr. author)
f) Università degli Studi di Torino, Italy

INTRODUCTION

The 2016 Central Italy earthquake sequence occurred in the central portion of the inner Apennine range, in the sector of the Laga and the Sibillini Mountains. These mountains have a complex geological history characterized by multiple phases of tectonic deformation (Falcucci et al. 2018, Galadini et al. 2018). Despite a lack of historical seismicity, the challenging task of geologic studies to identify locations of active fault segments, long-term fault behavior and kinematic characteristics, and the timing of past ruptures within the Laga and Sibillini Mountains had been undertaken before the 2016 events (e.g., Boncio et al. 2004, Calamita and Pizzi 1992, Cello et al. 1997, Galadini and Galli 2000, 2003). As a result, surface rupture data gathered following these events provide an excellent opportunity to eval- uate the effectiveness of these studies, particularly in regard to locations of rupture, changes in rupture patterns across previously mapped segment boundaries, as well as segmentation of seismogenic sources and seismic source parametrization.

The surface expression of the Mt. Vettore–Mt. Bove fault system is clearly visible on the southern ridge and western flank of the Mt. Vettore–Mt. Bove Massif within the Sibillini Mountains. On the southern and western flanks of Mt. Vettore, the fault trends approximately 30° west of north, whereas the trend is nearly northward on the north flank. Galadini and Galli (2003) mapped a complex zone of three major normal fault splays on the western slope of Mt. Vettore. Beginning at the base of the mountain on the west side, a normal fault occurs near the Castelluccio larger Quaternary basin margin (also known as Piano Grande basin). The basin represents a tectono-karstic depression, the shape (morphology) of which evolved in the Quaternary, as it was buried by continental deposits while being affected by both fault activity and the dynamics of a karstic system (Lippi Boncambi 1947). Therefore, the present setting of the Castelluccio basin cannot be related just to fault activity. Moving east, a second fault occurs mid-slope, followed by the upper (eastern) fault. The eastern upper normal fault runs along the southern and western upper flank of a subsidiary peak of Mt. Vettore called "Cima del Redentore." This fault trace is clearly visible from the Castelluccio basin and it is commonly called "Cordone del Vettore." Pierantoni et al. (2013) also mapped three potential faults in this zone, with an oblique normal fault between the western basin-edge fault and eastern upper-slope fault. The fault system continues northwesterly towards Mt. Bove, where several faults have been mapped.

Figure 1 shows the locations of the observed surface ruptures. The M6.1 24 August 2016 earthquake rupture produced clearly observable normal-mechanism displacements on the southern and western slopes of Mt. Vettore, along the Cordone del Vettore splay (EMERGEO 2016, GEER 2016). The M5.9 26 October event resulted in limited visible movements in the area of Mt. Bove, which is north of the fault intervals ruptured in the other two events (i.e., north of 42.90° in Figure 1). The M6.5 30 October earthquake greatly increased the observable normal-mechanism displacements in the areas affected by the 24 August event in both magnitude and length of rupture. The observed surface ruptures from these three events are nearly coincident with fault segments mapped before the 2016–2017 earthquake sequence.

Following this introduction, we review the regional geologic setting and pre-event geo- logic mapping studies in the subject region. We then describe the reconnaissance approach undertaken by the GEER team (including Italian collaborators), which included ground- based mapping and use of aerial imagery. The outcomes of the mapping are then described in two sections describing the general locations of rupture as observed following the different mainshocks and details on measured displacements and their locations. We conclude with a comparison of measured displacements to an empirical model. Further details of the surface rupture reconnaissance are contained in Chapters 2 of GEER (2016, 2017).

Previous publications describe surface displacements mapped following the 24 August earthquake (EMERGEO 2016, Pucci et al. 2017) and the 30 October earthquake (Civico et al. 2018, Villani et al. 2018), the latter of which are cumulative across multiple events.

STRUCTURAL SETTING AND PRIOR GEOLOGIC MAPPING

Bedrock exposed in the Laga and Sibillini Mountains belongs to a multideformed Mesozoic–Cenozoic sedimentary sequence (Umbria–Marche pelagic sequence, mainly limestone to marls), which experienced several tectonic phases prior to the Quaternary seismogenic one (e.g., Calamita et al. 1994, Falcucci et al. 2018, Ghisetti and Vezzani 1999, Lavecchia et al. 1994). Post-orogenic Quaternary and seismogenic active normal faults affect the Neogene Apennine fold-and-thrust belt (Figure 2), which was preceded by Triassic, Jurassic, Cretaceous–Paleogene, and Miocene extension (Castellarin et al. 1978, Centamore et al. 1971, Elter et al. 1975, Falcucci et al. 2018, Marchegiani et al. 1999, Patacca and Scandone, 1989). This succession of tectonic events, not always coaxial and with different kinematics, produced highly fractured rock masses and complex zones with multi-reactivated or crosscutting faults. In particular, the geological evolution of the region seems to have been deeply influenced by the multiphase activity of the Ancona–Anzio Line, a lithospheric dis- continuity whose kinematic history shaped the structural setting of the region since the Meso- zoic to the present (Falcucci et al. 2018).

An early official geologic map, prepared by Scarsella, identified different types of faults in the Sibillini Mountains region (Servizio Geologico d'Italia 1941). This map identified structures defined as "visible fractures and their hypothetical extension" that correspond well to the normal faults shown in Figures 1 and 2. Part of the Cordone del Vettore fault was mapped along the Mt. Vettore western slope at the same elevation as the currently mapped subsegment. Also, the Mt. Vettoretto fault splay was identified. Other synthetic and antithetic primary and secondary faults were also mapped in the areas of Mt. Porche, Mt. Bove, and Ussita village.

The first detailed geological-structural study to identify and map recent and active faults in the Sibillini Mountains area was presented by Calamita et al. (1992) and Calamita and Pizzi (1994). The latter describes geometric, kinematic, and relative chronology data along with detailed geologic structure. These works identified the active Mt. Vettore–Mt. Bove normal fault system and evaluated associated segment lengths. These studies describe a fault system about 27 km in length. The north boundary consists of a progressive reduction of throws along faults near Ussita and Cupi villages. The south terminus is quite sharp and abuts the oblique structural barrier of the Sibillini Mountains Miocene–Pliocene thrust, which, in turn, positively inverted (i.e., changed the direction of slip to thrust) the aforemen- tioned Ancona–Anzio Line (Falcucci et al. 2018, Pizzi and Galadini 2009). The system com- prises several NNW–SSE-trending, kilometers-long subparallel primary and secondary fault splays, both synthetic and antithetic, with oblique transfer fault segments and en-échelon patterns. Quaternary normal faults and active normal faults were also further distinguished based on relative chronologies inferred by structural and morphotectonic criteria.

Fault kinematics were described by Calamita and Pizzi (1994), who identified a major NNW-SSE fault system showing a normal kinematic or a very slight strike-slip component, and two minor fault sets oriented in the E-W and N-S directions. The first set shows both dextral transtensive and pure normal kinematics. The second set probably developed as trans- fer faults and/or reactivating pre-existing structures, and show sinistral oblique kinematics. The Mt. Vettore–Mt. Bove fault system kinematics were reinterpreted by Cello et al. (1997), who associated the activity of the seismogenic fault to a strike-slip regional stress field. Pierantoni et al. (2013) re-mapped the area based on a review of the existing geological maps, including the Geological Map of the Marche Region (Regione Marche 2001). A complex arrangement of primary and secondary normal faults, with both subparallel and en-échelon segments, were represented in the 2013 map and related geological cross sections, although no data about chronologies and fault activity were provided. Geological field data and paleoseismological trenches by Galadini and Galli (2003) revealed active faults affecting the Quaternary deposits within the Castelluccio basin (Figure 3).

Detailed mapping of the Mt. Vettore–Mt. Bove fault system showed that most of the normal-to-transtensive features produce active and capable normal faulting—that is, fault activation and surface displacement in the last 0.8 Myr (Galadini et al. 2012).

RECONNAISSANCE APPROACH

We undertook multiphase reconnaissance in which detection and measurement of surface fault rupture following the earthquake events consisted of three principal elements:

- General recognition of fault segments with and without surface rupture, which for the present work, was based principally on visual observation by geologists.
- Detailed mapping of surface rupture locations and direct measurement of displacements using rulers and tape measures.
- Imaging of the deformed ground surface near the fault using (1) unmanned aerial vehicles (UAVs) and (2) terrestrial light detection and ranging (LiDAR).

Figure 1 shows the broad area in which both observations of rupture locations and detailed mapping/imaging were undertaken. Detailed mapping following the first two events was based solely on accessing the fault on the ground and recording locations of rupture and amounts and directions of slip. This approach was supplemented with aerial imagery follow- ing the third (30 October) event. We found the use of aerial imagery to be effective, parti- cularly in steep terrain where ground access is challenging. On the other hand, in areas of localized slope instabilities (e.g., landslides, compaction of talus debris, fissures in thin soil overburden over shallow rock) occurring in the same region as surface rupture, accurate inter- pretation benefits considerably from field inspections by experienced geologists. This was occasionally the case at the bottom of ravines, gullies, or couloirs, or in dense vegetation.

LiDAR data were collected using the terrestrial laser scanning method (Bellian et al. 2005, Frei et al. 2004). The scanner was placed on a tripod and its GPS location recorded. A point cloud of coordinates visible to the scanner was collected and registered with the other scans in the same area.

Point-cloud data from the UAV were processed using a multistage process. First, a flight plan was selected to overfly the fault and collect downward-looking photographs using a Phantom 4 UAV quad-copter. Images were collected with minimum 80% overlap and 80% side-lap coverage to ensure common features in adjacent images. Using cloud computing software from Dronedeploy, and workstation-based software from Agisoft, the down- ward-looking images were aligned using hard features common to multiple photographs. Images were first aligned crudely, and then a sequence of higher-level alignments improved the model and established tight relationships between adjacent images. The structure- from-motion method computes angular separations between objects visible in overlapping images. The scale and location of the objects are determined by knowing the location of each photograph from the photo metadata GPS location. That is, the GPS-tagged photographs from the drone provided the scale for the model. The imagery was then used to process a dense point cloud and a three-dimensional (3-D) mesh triangular irregular network surface. The same aligned imagery was used to construct a precise orthomosaic of the scanned area.

A method was developed to merge point-cloud data from UAV imagery and the 3-D terrestrial laser scanner to record offsets along the Mt. Vettore–Mt. Bove fault system. The two datasets were merged using the software ISITE-Studio (Maptek company). The advantage of merging data is that the LiDAR data set is presumably more precise regarding pixel location, whereas the UAV data have a more accurate color representation for each pixel because of the direct relationship between the point cloud and the orthomosaic image.

Rupture offsets were measured in the 3-D orthomosaic using elevation difference between the top and bottom of visible planar surfaces. These are compared to GPS-located hand measurements of displacement.

GENERAL SURFACE RUPTURE OBSERVATIONS

The three mainshocks collectively produced surface rupture along most of the known and previously mapped normal fault strands on the southern and western slopes of the Mt. Vettore–Mt. Bove Massif. Figure 1 shows the general locations of surface rupture in relation to the finite fault models recommended by Galadini et al. (2018).

The M6.1 24 August event produced surface rupture that extended approximately 5 km north of the southern terminus of the Mt. Vettore–Mt. Bove fault system. Fault displacements of 0–35 cm (average of 12 cm) occurred in the down-dip direction, and horizontal cracks were opened. These fault displacements were observed at tens of sites that include bedrock exposures on both sides of the fault and colluvium and soil near to or adjacent to the bedrock fault plane. Limited observations were made following the 26 October event, which do not include detailed mapping, as a result of the short time window between this event and the subsequent M6.5 30 October event. Nonetheless, observations establish the presence and magnitude of surface rupture and its extent north of the August rupture (Figure 1).

Following the 30 October event, several phases of reconnaissance were performed that establish the fault segments on which rupture was and was not observed, and which provide details on the amounts and distributions of slip in some areas. This rupture began at the south end of the Mt. Vettore–Mt. Bove fault system, exactly coinciding to the south with the southernmost ruptures caused by the 24 August event, and continued north to partially overlap or increase the rupture from the 26 October event. As described below, detailed mapping in the southern part provides cumulative maximum tectonic displacements of up to about 180 cm. Inclement weather prevented full mapping of fault rupture after the 30 October event. Approximately the southern half of the rupture of the 30 October event was observed before winter snows.

Except for a few short surface cracks, sometimes having a curved trend in plan view and clearly relatable to gravitational phenomena, all of the surface ruptures occurred along fault planes that became freshly exposed (Figures 4–6). No visible ground cracks were detected even along steep slopes, where carbonate debris rested along the mountain flanks. This indi- cates that surface ruptures are almost exclusively associated with tectonic displacement and that gravitational mass movements were relatively minor (Albano et al. 2016), in contrast to some other interpretations (Huang et al. 2017). Figure 4 shows an example of surface rupture associated with a known splay of the Mt. Vettore–Mt. Bove fault system. Figure 4a compares the long-term geological downthrow based on displacement of the limestone sequences, and the coseismic offset caused by the 24 August and 30 October events. This area was the northern limit of UAV imaging acquired December 2016.

Occasionally, rupture strands displayed en-échelon arrangements, mostly with dextral stepover. Figure 5 shows this from the Mt. Vettoretto fault splay where connecting/transfer faults were identified in between the stepped ruptures. Where the ruptures affected loose soils, it resulted in distributed deformations, with offset split into additional strands.

In some areas, surface faulting occurred along previously unmapped fault strands; this was due to locally subdued geomorphic expression of the fault strands that prevented prior recognition and mapping. Figure 6 shows this behavior in the area of Mt. Porche.

From a geometric viewpoint, most of the ruptures were straight and crossed any morphology or terrain, even where the slope gradient was high. Figure 7 shows generally strait ruptures along steep terrain. Figure 8 shows similar geometry of the rupture from a UAV imaging derived 3-D orthomodel of the areas in Figures 4 and 5. The rupture surface of the western splay is shown in white, while the yellow lines in Figure 8 are primary rupture on the Cordone del Vettore fault, including some step-over at the transition from the south face to the southwest face of the Massif. Figure 9 shows the Piano Grande fault splay, which is the western-most splay of the Mt. Vettore–Mt. Bove fault system in the area of the Mt. Vettore Massif. This splay was trenched by Galadini and Galli (2003). We found ground rupture along this splay, with vertical throw of up to 18 cm. A composite orthomosaic of the Piano Grande fault is presented in Figure 10, composed of integrated UAV based on structure-from-motion data and LiDAR imaging point clouds.

The detailed observations of fault slip in several areas provide insight into which among several previously mapped strands can be considered as the main fault that defines the edge of the footwall, and which are strands within the hanging wall. In the case of the Mt. Vettore Massif, both the M6.1 and the M6.5 events produced maximum extensional strain along the Cordone del Vettore fault. Our interpretation is that the relatively modest additional slip on the western splays at the Mt. Vettore mid-slope and Castelluccio basin (Figures 3, 4, and 8) are synthetic features in the hanging wall. In the Mt. Porche–Palazzo Borghese area, the fault strand at higher elevation (F1 in Figure 6a), previously considered a splay or a secondary fault, showed the major coseismic throw (60–95 cm) in the NNW-SSE direction over a length of at least 2.5–3 km. These movements occurred on some newly formed or previously unrecognized fault segments (Figure 6 and 7).

DETAILED MAPPING OF SURFACE RUPTURE DISPLACEMENTS

This section presents results of field mapping conducted in the period August–September 2016 following the M6.1 24 August 2016 earthquake, and in the period November–December 2016 following the 26 and 30 October events.

M6.1 24 AUGUST EVENT

We made detailed hand measurements along the southern third of the Mt. Vettore–Mt. Bove fault system following the 24 August event. Figure 11 shows the locations of the three principal fault splays as described above, along with locations (and amounts) of measured displacements (EMERGEO 2016, Pucci et al. 2017). Displacements were observed only on the uppermost splay (Cordone del Vettore fault), over a distance of about 5.0 km. Where the fault plane was observed, the average measured strike was 158° with values ranging from 146° to 174°. The average fault dip was 46°, with a range of 36° to 62°. The measurement of 36° was potentially from an out-of-place block associated with the fault but detached. If we reject that value, then the average dip angle is 51.5°. The locations of mapped surface rupture were essentially coincident with the pre-event mapped locations of the Cordone del Vettore fault (Galadini and Galli 2003, Pierantoni et al. 2013).

OCTOBER EVENTS

Displacements produced by the 26 and 30 October events were measured in separate reconnaissance performed by a small Istituto Nazionale di Geofisica e Vulcanologia (INGV) team deployed following the 26 October event, and then by a much larger GEER team deployed following the 30 October event.

M5.9 26 October Event

After the M5.9 26 October event, field investigations were performed in the epicentral area, along the northern sector of the Mt. Vettore–Mt. Bove fault system trace, to look for possible evidence of surface faulting. We surveyed the area between Cupi to the north and Casali and Frontignano to the south. The fault system in this area consists of a main fault trace and a few synthetic strands.

In the area of Cupi, the Mt. Vettore–Mt. Bove fault system crosses a gently northwest dipping erosional land surface onto the carbonate bedrock (Figure 12). The landform is thought to have been originally formed nearly horizontally and next to an ancient (Pleistocene–early Quaternary in age) valley bottom, with the present slope reflecting base displacement associated with faulting, since the early Quaternary that can be estimated as roughly 200 m–300 m. Geomorphic features similar to those in this sector appear elsewhere in the central Apennines (e.g., Fubelli et al. 2009). Indeed, on the hanging wall, the land surface occurs between 920 m and 1,150 m above sea level (in the area of Cupi), whereas on the footwall, ground elevations are between ~1,200 m and 1,500 m above sea level.

We found evidence of reactivation of this part of the Mt. Vettore–Mt. Bove fault system following the 26 October event, in the form of ground cracks at the base of the fault scarp with vertical offsets of 10–20 cm (Figure 13). We made these observations at the contact between limestone in the footwall and scree that had accumulated at the base of the fault scarp. In the area of Frontignano, a 10- to 15-cm-high freshly exposed free face was observed at the base of a secondary synthetic splay of the fault, parallel to the main fault, which, conversely, showed no evidence of reactivation (the main fault here reactivated with the 30 October 2016 event, as described below).

M6.5 30 October Event

The 30 October event ruptured a 15-km-long section of the Mt. Vettore–Mt. Bove fault system. The southernmost 5 km of the ruptured fault had previously ruptured in the 24 August event. Because surface rupture observations made at a point in time represent the cumulative slip from prior events, slip resulting from the 30 October event is evaluated by differencing of multi-epoch displacement measurements. The detailed by-hand mapping conducted following the 24 August event for the southern portion of the Mt Vettore–Mt. Bove fault system provides baseline displacements that can be subtracted from those mea- sured in December 2016. Those differentials are attributed to the 30 October event because the 26 October event ruptured distinct segments north of the August rupture.

Figure 14 shows a location near the south end of the fault rupture, at road SP477, where multi-epoch photographs and measurements show the increase of slip in these areas from the 24 August event to the 30 October event. Figures 15–17 show three additional locations where displacements can be compared in soil overburden, an eroded channel, and the face of a rock slope. Additional multi-epoch photos showing incremental slip that occurred between 24 August and 30 October are shown in Figures A1–A4 in the online Appendix. The rock face shown in Figure 17 is an exposure of the Cordone del Vettore fault plane, on which recent slip is evident from discoloration.

At a few sites, gravitational movements of the scree (talus debris) at the base of the Cordone del Vettore scarp or local coseismic subsidence may have increased the fault downthrow; at the location in Figure 18, the slip was 215 cm. This displacement is a locally high value, with neighboring areas a few meters away varying from about 130 to 180 cm. Overall, the mean fault offset was on the order of 140 cm, with minimum values of about 120 cm. This can be compared to the 12-cm average following the 24 August event. Therefore, the ≥200-cm local offset results from the sum of tectonic displacement, likely on the order of 130–170 cm and local nontectonic displacements, related to gravitational effects.

Figure 19 shows a northern sector of the fault system, near Frontignano, where no surface rupture occurred prior to the 30 October event. This area had 50-cm fault offset after the 30 October event (Figure 19b and inset). This is the northernmost surface rupture caused by this event, with ∼1-km overlap with the southernmost surface rupture caused by the studies; Commissione Tecnica per la Microzonazione Sismica 2015), in which maximum shear zone widths around faults are often taken as 160 m.

Figure 20 compares co-located hand measurements of surface fault displacements as a function of location (latitude) for reconnaissance performed following the 24 August and 30 October events. The displacement differences shown in these plots can be attributed to the 30 October event, which are much larger than those from 24 August. As observed by others (e.g., Wells and Coppersmith 1994), offset increased towards the center of the rupture (i.e., to the north in Figure 20).

As shown in Figures 4–6 (and summarized in Figure 1), locations of observed surface rupture features during the sequence generally conform well with the pre-event mapped locations of the main fault (Cordone del Vettore) and western splays at the Mt. Vettore mid-slope and Castelluccio basin. However, as described earlier (and highlighted in Figure 6), there are exceptions of observed rupture on new or previously unrecognized faults.

Because the reconnaissance performed following the 30 October event included both hand measurements of surface rupture and the development of point clouds along the fault from which displacements can be inferred, the data provide a means by which to com- pare these outcomes. Figure 21 provides such a comparison of displacements measured along the primary (highest elevation) segment of the Mt. Vettore–Mt. Bove fault system. These displacement measurements were made along the portions of Mt. Vettore that are on the west face of the ridge and on the branch descending the ridge towards SP477. The 3-D model in these areas is based on UAV point-cloud data, and the displacements were measured from the model using the program Dronedeploy. Viewing the data as a whole, there is no evidence of bias of one measurement type relative to the other. Where significant discrepancies occur, they typically involve local regions with poor lines of sight for UAV, such as areas of thick vegetation and the bottoms of gullies, ravines, and couloirs. Several such instances are marked in Figure 21. This admittedly small-scale validation of UAV-based measurements of surface rupture offsets may serve to encourage the use of such techniques in future recon- naissance, especially in areas of limited accessibility.

Postseismic Slip

Some areas along the fault have experienced additional slip (up to ∼15% of coseismic throw) over an approximately one-year period following the reconnaissance in November 2016 (related to the 30 October event). The cause of these additional displacements is unknown. Photographic evidence is provided in Figures A5 and A6 in the online Appendix.

COMPARISON TO EMPIRICAL MODELS

We compile summary statistics on the surface rupture for comparison with model pre- dictions by Wells and Coppersmith (1994), with minor modification by Wells (2015). A similar comparison was presented previously for the 24 August event by Pucci et al. (2017).

The comparison is straightforward for the ruptures caused by the 24 August and 26 October events. For the 30 October event, we use data only from selected locations where both pre- and post-event surface rupture displacements were measured. Figure 22a and 22b shows surface and subsurface rupture lengths versus magnitude, respectively. Surface rupture lengths are based on the data presented here, whereas subsurface rupture lengths are based on trimmed finite fault models presented in Galadini et al. (2018). In both cases, data from the 2016 Central

Italy earthquake sequence compare well with model predictions. Figure 22c and 22d shows average and maximum displacements versus magnitude, respectively; average and maximum displacements plot at or below model predictions.

CONCLUSIONS

We investigated surface rupture of the Mt. Vettore–Mt. Bove fault system using both conventional field mapping and UAV/LiDAR imaging. The multiphase approach, as implemented following the October events, was successful in that: (1) additional rupture surfaces were rapidly identified by remote imaging over large areas of difficult terrain; and (2) on steeply sloping ground, UAV/LiDAR imaging captures all scarps and features regardless of causation from fault rupture or local slope instability, which can then be evaluated by field mapping to avoid mis-identifications of surface faulting. Future fault rupture reconnais- sance efforts, especially in steep terrain, may benefit from use of a similar multiphase approach.

Due to extensive field mapping that preceded the earthquake sequence, the surface rupture observations provide an opportunity to evaluate the accuracy of "pre-earthquake" mapped fault locations. Most of the observed coseismic ruptures reactivated previously mapped fault planes, rejuvenating the related scarps. In particular, field surveys performed soon after each event highlight the twofold reactivation of most of the length of the Mt. Vettore–Mt. Bove fault system. There are four significant practical outcomes of these findings:

1. The maps were broadly accurate. This suggests that geologic-structural and morpho-tectonic field studies, which were the basis for the maps, can be effective for detecting fault systems and distinguishing active from long-inactive (e.g., pre-Middle-Lower Pleistocene) faults. There were exceptions to the accurate pre-event mapping, mostly involving newly formed or previously unrecognized secondary fault strands that rup- tured in the M6.5 30 October event (e.g., Figure 6). This typically resulted from por- tions of faults having been concealed by overlying sediments.

2. Secondary faulting was generally relatively minor, which is in contrast to significant secondary fault effects in normal fault terrains elsewhere (Youngs et al. 2003). It is not

presently known whether this is a unique feature of the Mt. Vettore–Mt. Bove fault system or a more general feature of normal faults in the central Apennines. An excep- tion is portions of the fault with multiple strands that had been mapped pre-event.

3. Fault zone widths were generally quite narrow, on the order of a few meters or less approximately along strait fault sections. Exceptions are en-échelon step-over regions and areas with multiple fault splays, discussed below.

4. As described further in Galadini et al. 2018, the southern terminus of the Mt. Vettore–Mt. Bove fault system occurs in a complex zone that transitions to the south to the separate Amatrice fault (shown in Figure 2). The extent of surface rupture conformed well with this mapping, confirming the segment boundary in this region.

These findings have relevance for microzonation efforts in Italy intended to guide land management in areas of active and capable faults (Commissione Tecnica per la Microzonazione Sismica 2015). Once an active and capable normal fault has been mapped, in a relatively detailed (Level 3) study, the criteria identify hazard zones 160 m in width, with a 30-m setback zone where development should be made following prescriptions. That set back zone is asymmetrically shaped around the fault trace (footwall/hanging wall ratio = 1:4). These setback criteria are conservative with respect to our observations, which generally indicated narrow primary fault ruptures. However, the presence of newly formed or previously unrecognized fault strands in areas where sediments overlie the fault may suggest the use of broader setback and hazard zones in such areas to reflect mapping uncertainty.

An important consideration in locating zones of surface rupture hazards from geologic-structural field mapping pertains to major fault splays (e.g., length > 0.5–1 km), which can occur on the hanging wall of active faults. Activation of such splays was not observed in the M6.1 August event or in the M5.9 October event, but did occur in the larger M6.5 event, as shown, for example, in Figures 3 and 8. While such ruptures on fault splays produce in effect a wide rupture zone (up to several kilometers), it is encouraging that the splay locations in addition to the main fault location had been identified pre-event. As a result, the experience from the 2016 surface rupture is that fault-specific detailed investigations can be effective for locating zones of rupture hazard from both principle fault structures and major secondary features.

ACKNOWLEDGMENTS

The GEER Association is supported by the National Science Foundation (NSF) through the Geotechnical Engineering Program under Grant Number CMMI-1266418. Any opinions, findings, and conclusions or recommendations expressed in this material are those of the authors and do not necessarily reflect the views of the NSF. The GEER Association is made possible by the vision and support of the NSF Program Directors: Richard Fragaszy and the late Cliff Astill. GEER members also donate their time, talent, and resources to col- lect time-sensitive field observations of the effects of extreme events. This work was also partially supported by the Center for Unmanned Aircraft Systems (C-UAS), a National Science Foundation Industry/University Cooperative Research Center (I/UCRC) under NSF Award Number CNS-1650547 along with significant contributions from C-UAS indus- try members. UAV flight permits and access to fault rupture areas were obtained thanks to the help of Paola Pagliara and Paola Bertuccioli of Dipartimento della protezione civile (DPC).

APPENDIX

Please refer to the online version of this paper to access the supplementary material provided in the Appendix.

REFERENCES

Albano, M., Saroli, M., Moro, M., Falcucci, E., Gori, S., Stramondo, S., Galadini, F., and Barba, S., 2016. Minor shallow gravitational component on the Mt. Vettore surface ruptures related to MW 6, 2016 Amatrice earthquake, Annals of Geophysics 59, Fast Track 5.

Bellian, J. A., Kerans, C., and Jennette, D. C., 2005. Digital outcrop models: applications of terrestrial scanning LiDAR technology in stratigraphic modeling, Journal of Sedimentary Research, 75, 166–176.

Boncio, P., Lavecchia, G., and Pace, B., 2004. Defining a model of 3D seismogenic sources for Seismic Hazard Assessment applications: the case of central Apennines (Italy), Journal of Seismology 8, 407–425.

Bonini, L., Maesano, F., Basili, R., and Valensise, G., 2016. Imaging the tectonic framework of the Amatrice (Central Italy) earthquake sequence: New roles for old players?, Annals of Geo- physics 59, doi.10.4401/ag-7229.

Calamita, F., Coltorti, M., Farabollini, P., and Pizzi, A., 1994. Le faglie normali quaternarie nella dorsale appenninica umbro-marchigiana: Proposta di un modello di tettonica di inversione, Studi Geologici Camerti 1, 211–225.

Calamita, F., and Pizzi, A., 1992. Tettonica quaternaria nella dorsale appenninica umbro-marchigiana e bacini intrappenninici associati, Studi Geologici Camerti 1, 17–25.

Calamita, F., and Pizzi, A., 1994. Recent and active extensional tectonics in the southern Umbro-Marchean Apennines (Central Italy), Memorie della Società Geologica Italiana 48, 541–548.

Calamita, F., Pizzi, A., and Roscioni, M., 1992. I "fasci" di faglie recenti ed attive di M. Vettore–M. Bove e di M. Castello–M. Cardosa (Appennino Umbro–Marchigiano), Studi Geologici Camerti 1, 81–95.

Calamita, F., Satolli, S., Scisciani, V., and Pace, P., 2011. Contrasting styles of fault reactivation in curved orogenic belts: Examples from the Central Apennines, GSA Bulletin 123, 1097–1111.

Castellarin, A., Colacicchi, R., and Praturlon, A., 1978. Fasi distensive, trascorrenze e sovrascorrimenti lungo la linea Ancona-Anzio dal Lias al Pliocene, Geologica Romana 17, 161–189.

Cello, G., Mazzoli, S., Tondi, E., and Turco, E., 1997. Active tectonics in the Central Apennines and possible implications for seismic hazard analysis in peninsular Italy, Tectonophysics 272, 43–68.

Centamore, E., Chiocchini, M., Deiana, G., Micarelli, A., and Pieruccini, U., 1971. Contributo alla conoscenza del Giurassico dell'Appennino umbro-marchigiano, Studi Geologici Camerti 1, 7–89.

Chiaraluce, L., Di Stefano, R., Tinti, E., Scognamiglio, L., Michele, M., Casarotti, E., Cattaneo, M., De Gori, P., Chiarabba, C., Monachesi, G., Lombardi, A., Valoroso, L., Latorre, D., and Marzorati, S., 2017. The 2016 Central Italy seismic sequence: a first look at the mainshocks, aftershocks, and source models, Seismological Research Letters 88, 757–771.

Civico, R., Pucci, S., Villani, F., Pizzimenti, L., De Martini, P. M., and Nappi, R., and the Open EMERGEO Working Group, 2018. Surface ruptures following the 30 October 2016 Mw 6.5 Norcia earthquake, Central Italy, Journal of Maps 14(2), 151–160.

Commissione Tecnica per la Microzonazione Sismica, 2015. Linee guida per la gestione del territorio in aree interessate da Faglie Attive e Capaci (FAC), Versione 1.0, Conferenza delle Regioni e delle Province Autonome – Dipartimento della Protezione Civile, Roma, Rome, Italy.

De Guidi, G., Vecchio, A., Brighenti, F., Caputo, R., Carnemolla, F., Di Pietro, A., Lupo, M., Maggini, M., Marchese, S., Messina, D., Monaco, C., and Naso, S., 2017. Brief communica- tion: co-seismic displacement on 26 and 30 October 2016 (Mw D 5:9 and 6.5) – Earthquakes in Central Italy from the analysis of a local GNSS network, Natural Hazards and Earth System Sciences 17, 1885–1892.

Di Domenica, A., Petricca, P., Trippetta, F., Carminati, E., and Calamita, F., 2014. Investigating fault reactivation during multiple tectonic inversions through mechanical and numerical modeling: an application to the Central Apennines of Italy, Journal of Structural Geology 67, 167–185.

Di Domenica, A., Turtù, A., Satolli, S., and Calamita, F., 2012. Relationships between thrusts and normal faults in curved belts: new insight in the inversion tectonics of the Central-Northern Apennines (Italy), Journal of Structural Geology 42, 104–117.

Elter, P., Giglia, G., Tongiorgi, M., and Trevisan, L., 1975. Tensional and compressional areas in the recent (Tortonian to present) evolution of the Northern Apennines, Bollettino di Geofisica Teorica ed Applicata 65, 3–18.

EMERGEO, 2016. Coseismic effects of the 2016 Amatrice seismic sequence: First geological results, Annals of Geophysics 59, Fast Track 5, doi:10.4401/ag-7195.

Falcucci, E., Gori, S., Galadini, F., Fubelli, G., Moro, M., and Saroli, M., 2016. Active faults in the epi-central and mesoseismal Ml 6.0 24, 2016 Amatrice earthquake region, Central Italy, Methodological and seismotectonic issues, Annals of Geophysics 59, Fast Track 5.

Frei, E., Kung, J., and Bukowski, R., 2004. High-definition surveying (HDS): a new era in reality capture, in International Archives of Photogrammetry Remote Sensing and Spatial Informa- tion Science XXXVI-8/W2, 262–271.

Fubelli, G., Gori, S., Falcucci, E., Galadini, F., and Messina, P., 2009. Geomorphic signatures of recent normal fault activity versus geological evidence of inactivity: Case studies from the central Apennines (Italy), Tectonophysics 476, 252–268.

Galadini, F., Falcucci, E., Galli, P., Giaccio, B., Gori, S., Messina, P., Moro, M., Saroli, M., Scardia, G., and Sposato, A., 2012. Time intervals to assess active and capable faults for engi- neering practices in Italy, Engineering Geology 139–140, 50–65.

Galadini, F., Falcucci, E., Gori, S., Zimmaro, P., Cheloni, D., and Stewart, J. P., 2018. Tectonic setting of 2016-2017 Central Italy event sequence and observed source characteristics, Earthquake Spectra 34, 1557–1583. doi:10.1193/101317EQS204M.

Galadini, F., and Galli, P., 2000. Active tectonics in the Central Apennines (Italy) – Input data for seismic hazard assessment, Natural Hazards 22, 225–270.

Galadini, F., and Galli, P., 2003. Paleoseismology of silent faults in the Central Apennines (Italy): the Mt. Vettore and Laga Mts. faults, Annals of Geophysics 46, 815–836.

Geotechnical Extreme Events Reconnaissance (GEER) Association, 2016. Engineering Recon- naissance of the 24 August 2016 Central Italy Earthquake, Version 2 (P. Zimmaro and J. P. Stewart, eds.), Geotechnical Extreme Events Reconnaissance Association Report No. GEER-050B. doi:10.18118/G61S3Z.

Geotechnical Extreme Events Reconnaissance (GEER) Association, 2017. Engineering Reconnaissance following the October 2016 Central Italy Earthquakes, Version 2 (P. Zimmaro and J. P. Stewart, eds.), Geotechnical Extreme Events Reconnaissance Association Report No. GEER-050D. doi:10.18118/G6HS39.

Ghisetti, F., and Vezzani, L., 1999. Depth and modes of Pliocene-Pleistocene crustal extension of the Apennine (Italy), Terra Nova 11, 67–72.

Huang, M. H., Fielding, E. J., Liang, C., Milillo, P., Bekaert, D., Dreger, D., and Salzer, J., 2017. Coseismic deformation and triggered landslides of the 2016 MW 6.2 Amatrice earthquake in Italy, Geophysical Research Letters 44, 1266–1274.

Lavecchia, G., Brozzetti, F., Barchi, M., Menichetti, M., and Keller, J. V. A., 1994. Seismotectonic zoning in east-central Italy deduced from an analysis of the Neogene to present defor- mations and related stress fields, GSA Bulletin 106, 1107–1120.

Lavecchia, G., Castaldo, R., de Nardis, R., De Novellis, V., Ferrarini, F., Pepe, S., Brozzetti, F., Solaro, G., Cirillo, D., Bonano, M., Boncio, P., Casu, F., De Luca, C., Lanari, R., Manunta, M., Manzo, M., Pepe, A., Zinno, I., and Tizzani, P., 2016. Ground deformation and source geometry of the 24 August 2016 Amatrice earthquake (Central Italy) investigated through analytical and numerical modeling of DInSAR measurements and structural-geological data, Geophysical Research Letters 43, 12389–12398.

Lippi Boncambi, C., 1947. Idrologia sotterranea dell'altopiano del Castelluccio. Istituto di Mineralogia e Geologia dell'Università di Perugia, Perugia.

Marchegiani, L., Bertotti, G., Cello, G., Deiana, G., Mazzoli, S., and Tondi, E., 1999. Pre- orogenic tectonics in the Umbria-Marche sector of the Afro-Adriatic continental margin, Tectonophysics 315, 123–143.

Patacca, E., and Scandone, P., 1989. Post-Tortonian mountain building in the Apennines. The role of the passive sinking of a relic lithospheric slab, in The Lithosphere in Italy: Advances in Earth Science Research, Academia Nazionale dei Lincei, Rome, Italy, 157–176.

Pierantoni, P. P., Deiana, G., and Galdenzi, S., 2013. Stratigraphic and structural features of the Sibillini Mountains (Umbria-Marche Apennines, Italy), Italian Journal of Geosciences 132(3), 497–520.

Pizzi, A., 1992. Faglie recenti ed attive e origine delle depressioni tettoniche. Esempi dall' Appennino umbro–marchigiano, Tesi di dottorato, Università degli Studi della Calabria, Rende.

Pizzi, A., Di Domenica, A., Gallovič, F., Luzi, L., and Puglia, R., 2017. Fault segmentation as constraint to the occurrence of the main shocks of the 2016 Central Italy seismic sequence, Tectonics 36, 2370–2387.

Pizzi, A., and Galadini, F., 2009. Pre-existing cross-structures and active fault segmentation in the northern-central Apennines (Italy), Tectonophysics 476, 304–319.

Pucci, S., De Martini, P. M., Civico, R., Villani, F., Nappi, R., Ricci, T., Azzaro, R., Brunori, C. A., Caciagli, M., Cinti, F. R., Sapia, V., De Ritis, R., Mazzarini, F., Tarquini, S., Gaudiosi, G., Nave, R., Alessio, G., Smedile, A., Alfonsi, L., Cucci, L., and Pantosti, D., 2017. Coseismic ruptures of the 24 August 2016, Mw 6.0 Amatrice earthquake (Central Italy), Geophysical Research Letters 44, 2138–2147.

Regione Marche, 2001. Carta Geologica Regionale 1:10000, Progetti CARG e Obiettivo 5B. P.F. Regione Marche Giunta Regionale, via Gentile da Fabriano, 9 - 60125 Ancona, ITALY, available at: http://www.regione.marche.it/Regione-Utile/Paesaggio-Territorio-Urbanistica/ Cartografia/Repertorio/Cartageologicaregionale10000 (last accessed 13 October 2018).

Servizio Geologico d'Italia, 1941. Carta Geologica d'Italia alla scala 1:100.000, F°132

"Norcia," Ist. Poligrafico e Zecca dello Stato, Rome, Italy.

Villani, F., Civico, R., Pucci, S., Pizzimenti, L., Nappi, R., and De Martini, P. M., and the Open EMERGEO Working Group, 2018. A database of the post-30 October 2016 Norcia earthquake coseismic effects in Central Italy, Scientific Data 5, 180049.

Wells, D. L., 2015. Issues and approaches for estimating Mmax for earthquake sources in the basin and range province, in Proceedings of the Basin and Range Province Seismic Hazards Summit III: Utah Geological Survey Miscellaneous Publication 15-5, (W. R. Lund, ed.), DVD, Natural Resources Map & Bookstore, Salt Lake City, UT. ISBN: 978-1-55791-916-8.

Wells, D. L., and Coppersmith, K. J., 1994. New empirical relationships among magnitude, rupture length, rupture width, rupture area, and surface displacement, Bulletin of the Seismo- logical Society of America 84, 974–1002.

Youngs, R. R., Arabasz, W. J., Anderson, R. E., Ramelli, A. R., Ake, J. P., Slemmons, D. B., McCalpin, J. P., Doser, D. I., Fridrich, C. J., Swan, F. H., Rogers, A. M., Yount, J. C., Anderson, L. W., Smith, K. D., Bruhn, R. L., Knuepfer, P. L. K., Smith, R. B., dePolo, C. M., O'Leary, D. W., Coppersmith, K. J., Pezzopane, S. K., Schwartz, D. P., Whitney, J. W., Olig, S. S., and Toro, G. R., 2003. A methodology for probabilistic fault displacement hazard analysis (PFDHA), Earthquake Spectra 19, 191–219.

CAPTIONS

Figure 1. Map of surface fault rupture in the Sibillini Mountains, pre-event mapping of Mt. Vettore–Mt. Bove fault system (green), finite fault models for all three sequence events (from Galadini et al. 2018), observed surface ruptures, and locations of 3-D orthomodels shown in Figures 8 and 10.

Figure 2. (a) Location map of the area in (b). (b) Map of the relief and simplified structural map of the Central Apennines showing schematically the trace of the Quaternary and/or active normal fault systems affecting the axial zone of the chain and the main thrusts (after Boncio et al. 2004, Pizzi and Galadini 2009). Mt. Vettore–Mt. Bove (VBF) and Laga (LF) faults (marked blue lines) were involved in the 2016–2017 seismic sequence.

Figure 3. (a) Schematic of the southern sector of the Mt. Vettore–Mt. Bove fault system. (b) Schematic geological NE-SW trending cross section through the Quaternary/active normal faults bounding the Castelluccio Quaternary basin (Piano Grande). These faults recorded a maximum coseismic throw of 0.2 m on the 24 August M6.1 earthquake and on the order of 1.0–1.8 m (and very locally up to 2 m, probably increased by gravitational movements) during the 30 October M6.5 event.

Figure 4. (a) Scheme of the normal faults (from Pierantoni et al. 2013) and Quaternary/active normal faults (from Calamita et al. 1992, Pizzi 1992) mapped in the southernmost sector of the Mt. Vettore–Mt. Bove fault system (Cordone del Vettore area, see Figure 3). Coseismic ruptures occurred during both the 24 August and 30 October 2016 events. (b) Coseismic ruptures are visible in correspondence with the western splay bedrock fault scarp (white arrows) along which alluvial fan apexes are aligned.

Figure 5. (a) Normal faults (from Pierantoni et al. 2013) and Quaternary/active normal faults (from Calamita et al. 1992, Pizzi 1992) mapped in the southernmost sector of the Mt. Vettore–Mt. Bove fault system (Mt. Vettoretto area, see Figure 3). MST: Sibillini Mts thrust. (b) Sketch of the observed coseismic ruptures, which reflected the pre-existing en-échelon pattern of bedrock faults already mapped in the literature. Several NNW-SSE-trending en-échelon ruptures developed at the relay zone between the NW-SE-trending bedrock faults, suggesting incipient fault linkage. (c) Coseismic ruptures occurred during both the 24 August and 30 October 2016 events (white arrows). Complex surface rupture patterns and more distributed deformations characterized this portion of the fault, where no clear bedrock scarps outcrop and where active faults can be recog- nized due to the presence of

morphologic/geologic evidence, such as elongate depressions, sad- dles, and accumulation of rock debris at the base of periodically exposed bedrock-free faces.

Figure 6. (a) Normal faults (from Calamita et al. 1992, Pierantoni et al. 2013) mapped in the central sector of the fault system. The faults in this area did not show coseismic surface evidence after the 24 August and 26 October and were activated only during the 30 October event. Coseis- mic ruptures remarked the mapped bedrock faults (e.g., F1) both synthetic and antithetic, and new ruptures have been observed with continuity both northwest and southeast of Mt. Porche. (b) Geological cross section showing Quaternary/active normal faults. (c) Newly formed ruptures developed in correspondence of a saddle, northwest of the Mt. Porche bedrock fault plane. (d) Only a portion of the already mapped Mt. Porche fault has been reactivated after the 30 October event, and newly formed ruptures occurred along the slope.

Figure 7. Surface ruptures caused by the M6.5 30 October event along the Mt. Vettore western slope, indicated by white arrows, crossing any terrains and morphologies.

Figure 8. UAV based orthomosaic model of the SW face of the Mt. Vettore Massif, including the areas in Figures 4 and 5 after the 30 October earthquake, showing fault traces as mapped by UAV. Yellow lines denote primary fault rupture. White line indicates rupture of the mid-slope splay.

Figure 9. Piano Grande fault splay, affecting the Castelluccio plain, trenched by Galadini and Galli (2003). A Late Pleistocene–Holocene alluvial fan top surface is displaced by the fault strands (yellow dotted lines at different elevations across the fault). Surface rupture (up to 15–20 cm offset) along this structure occurred after the 30 October event.

Figure 10. Piano Grande fault rupture orthomosaic from composite LiDAR and UAV sensing data. Yellow line is the mapped fault rupture.

Figure 11. Relief map showing amounts of displacement (a) down-dip, and (b) horizontally (from crack openings), and histograms of measured displacements (EMERGEO 2016). Base map shows the three principal Mt. Vettore fault splays and other (relatively minor) splays. Inset shows exposed fault surface, including the increment exposed in the 24 August event between white dotted lines.

Figure 12. Google Earth image showing displacement of the erosional land surface (indicated by yellow arrows) across some fault splays (indicated by red lines) of the northern sector of the Mt. Vettore–Mt. Bove fault system.

Figure 13. Surface faulting (indicated by white arrows) along the northern segment of the Mt. Vettore–Mt. Bove fault system and a synthetic splay.

Figure 14. Comparative fault offset on the south face of Mt. Vettore at road SP477. (a) 2-cm vertical offset from the August event; and (b) 15-cm vertical offset from the October 2016 events. Horizontal offsets were 0 cm. Lat = 42.7971, Long = 13.2670.

Figure 15. Comparative fault offset on the south face of Mt. Vettore near road SP477. (a) 10-cm vertical offset from the 24 August event; and (b) 30-cm vertical offset following the 30 October 2016 event. Horizontal offsets were 0 and 2 cm. Lat = 42.79795°, Long = 13.26607°.

Figure 16. Comparative fault offset at the northern terminus of the Mt. Vettoretto fault branch, between (a) the 24 August event and (b) the 30 October event. Lat = 42,8075°, Long = 13.2632°.

Figure 17. Free face exposed at the base of the Cordone del Vettore fault scarp. Here, the twofold exposures of the fault plane owing to the 24 August (marked by yellow lines) and 30 October events (marked by red lines) are visible.

Figure 18. Local gravitational movements of the scree accumulating at the base of the fault scarp increased the downthrow at this location from 130 cm to up to 215 cm (walking sticks rest on the free face).

Figure 19. (a) Major fault scarp of the Mt. Vettore–Mt. Bove fault system, near Frontignano. No surface rupture occurred at this location after the 26 October 2016 event; and (b) offset of about 50 cm was observed after the 30 October 2016 event.

Figure 20. Distribution of incremental and cumulative fault offsets for the southern half of the Mt. Vettore–Mt. Bove fault system. All data in this figure are from hand measurements.

Figure 21. Surface fault rupture displacements from August–October event sequence as evaluated from hand measurements in the field and UAV-based 3-D model.

Figure 22. Observed rupture lengths and displacements against magnitude compared with model predictions by Wells (2015) (slight modification of Wells and Coppersmith 1994). (a) Surface rupture length (km), (b) subsurface rupture length (km), (c) average displacements (m), and (d) maximum displacements (m).

FIGURES

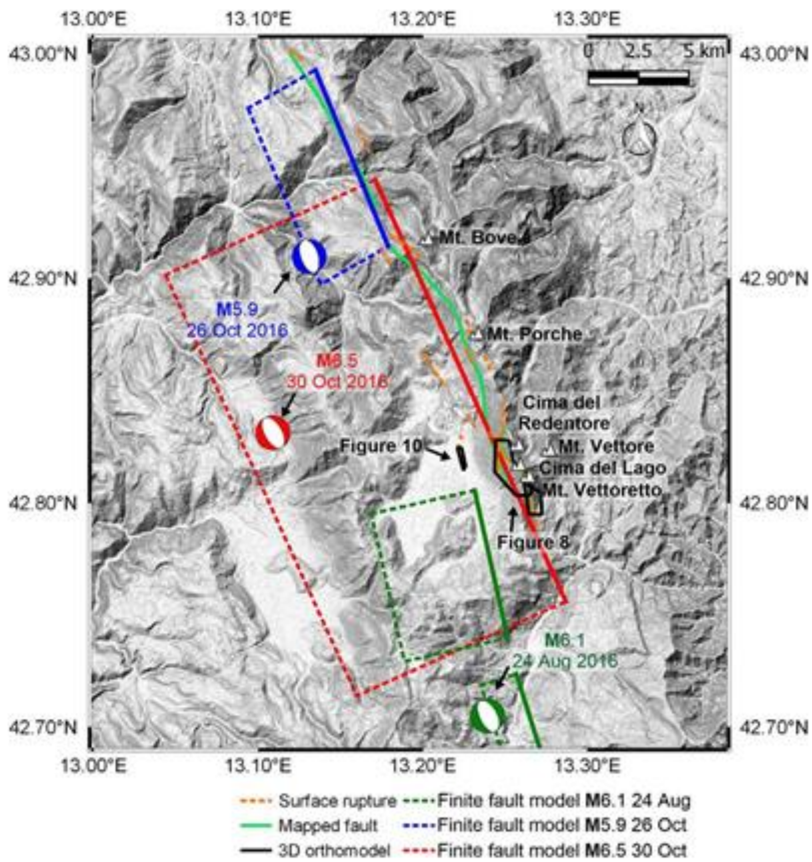

Figure 1

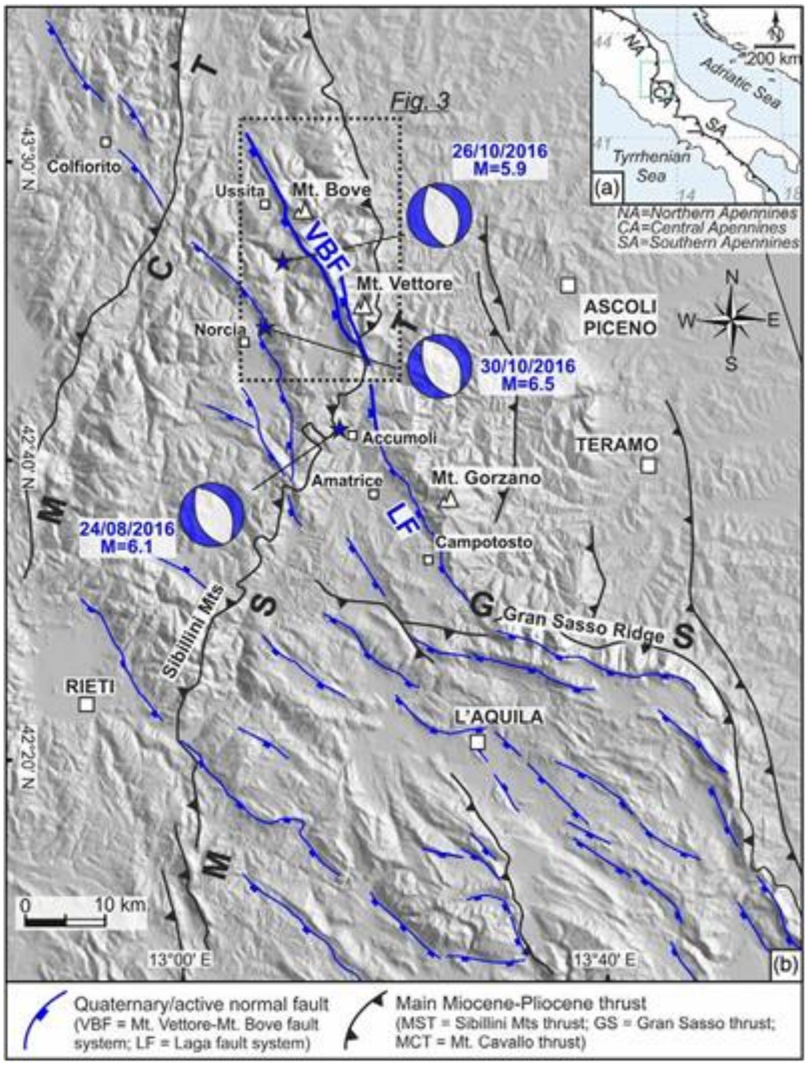
Fig. 3
26/10/2016
M=5.9
30/10/2016
M=6.5
24/08/2016
M=6.1
Colfiorito
Ussita
Mt. Bove
VBF
Mt. Vettore
Norcia
Accumoli
Amatrice
Mt. Gorzano
LF
Campotosto
ASCOLI
PICENO
TERAMO
Gran Sasso Ridge
Sibillini Mts
RIETI
L'AQUILA
43°30' N
42°40' N
42°20' N
13°00' E
13°40' E
0
10 km
(b)
NA
CA
SA
Adriatic Sea
Tyrrhenian
Sea
200 km
(a)
NA=Northern Apennines
CA=Central Apennines
SA=Southern Apennines
N
S
W
E
Quaternary/active normal fault
(VBF = Mt. Vettore-Mt. Bove fault system; LF = Laga fault system)
Main Miocene-Pliocene thrust
(MST = Sibillini Mts thrust; GS = Gran Sasso thrust; MCT = Mt. Cavallo thrust)

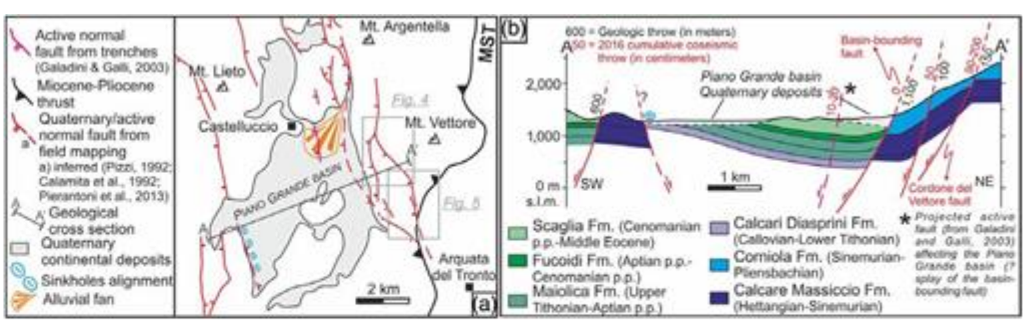
Active normal fault from trenches (Galadini & Galli, 2003)
Miocene-Pliocene thrust
Quaternary/active normal fault from field mapping
a) inferred (Pizzi, 1992; Calamita et al., 1992; Pierantoni et al., 2013)
Geological cross section
Quaternary continental deposits
Sinkholes alignment
Alluvial fan
Mt. Argentella
Mt. Lieto
Castelluccio
Mt. Vettore
Fig. 4
Fig. 5
PIANO GRANDE BASIN
MST
Arquata del Tronto
2 km
(a)
(b)
600 = Geologic throw (in meters)
50 = 2016 cumulative coseismic throw (in centimeters)
Basin-bounding fault
Piano Grande basin Quaternary deposits
A
A'
2,000
1,000
0 m s.l.m.
SW
NE
1 km
Cordone del Vettore fault
Scaglia Fm. (Cenomanian p.p.-Middle Eocene)
Fucoidi Fm. (Aptian p.p.-Cenomanian p.p.)
Maiolica Fm. (Upper Tithonian-Aptian p.p.)
Calcari Diasprini Fm. (Callovian-Lower Tithonian)
Corniola Fm. (Sinemurian-Pliensbachian)
Calcare Massiccio Fm. (Hettangian-Sinemurian)
Projected active fault (from Galadini and Galli, 2003) affecting the Piano Grande basin (? splay of the basin-bounding fault)

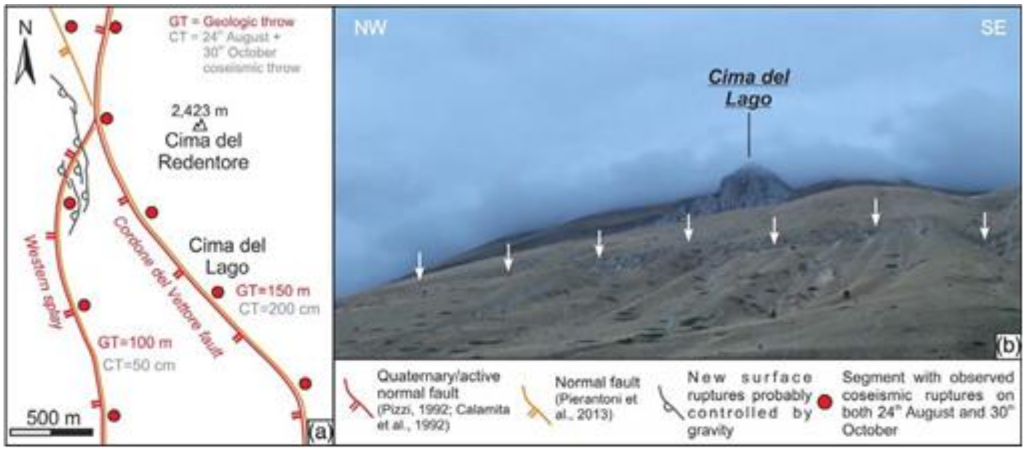
N
GT = Geologic throw
CT = 24th August + 30th October coseismic throw
2,423 m
Cima del Redentore
Cima del Lago
GT=150 m
CT=200 cm
Western splay
Cordone del Vettore fault
GT=100 m
CT=50 cm
500 m
(a)
NW
SE
Cima del Lago
(b)
Quaternary/active normal fault (Pizzi, 1992; Calamita et al., 1992)
Normal fault (Pierantoni et al., 2013)
New surface ruptures probably controlled by gravity
Segment with observed coseismic ruptures on both 24th August and 30th October

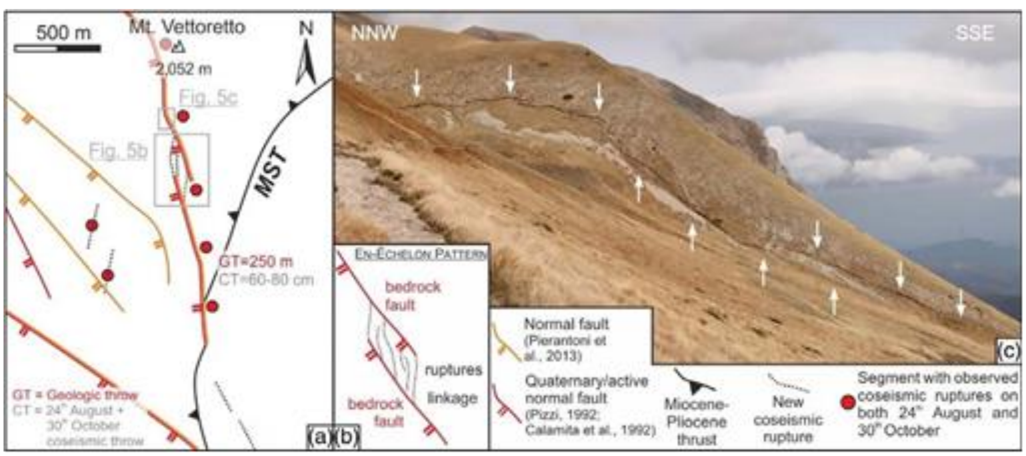
500 m
Mt. Vettoretto
2,052 m
N
Fig. 5c
Fig. 5b
MST
GT=250 m
CT=60-80 cm
GT = Geologic throw
CT = 24th August + 30th October coseismic throw
(a)
(b)
EN-ÉCHELON PATTERN
bedrock fault
ruptures linkage
bedrock fault
NNW
SSE
(c)
Normal fault (Pierantoni et al., 2013)
Quaternary/active normal fault (Pizzi, 1992; Calamita et al., 1992)
Miocene-Pliocene thrust
New coseismic rupture
Segment with observed coseismic ruptures on both 24th August and 30th October

Figure 5.

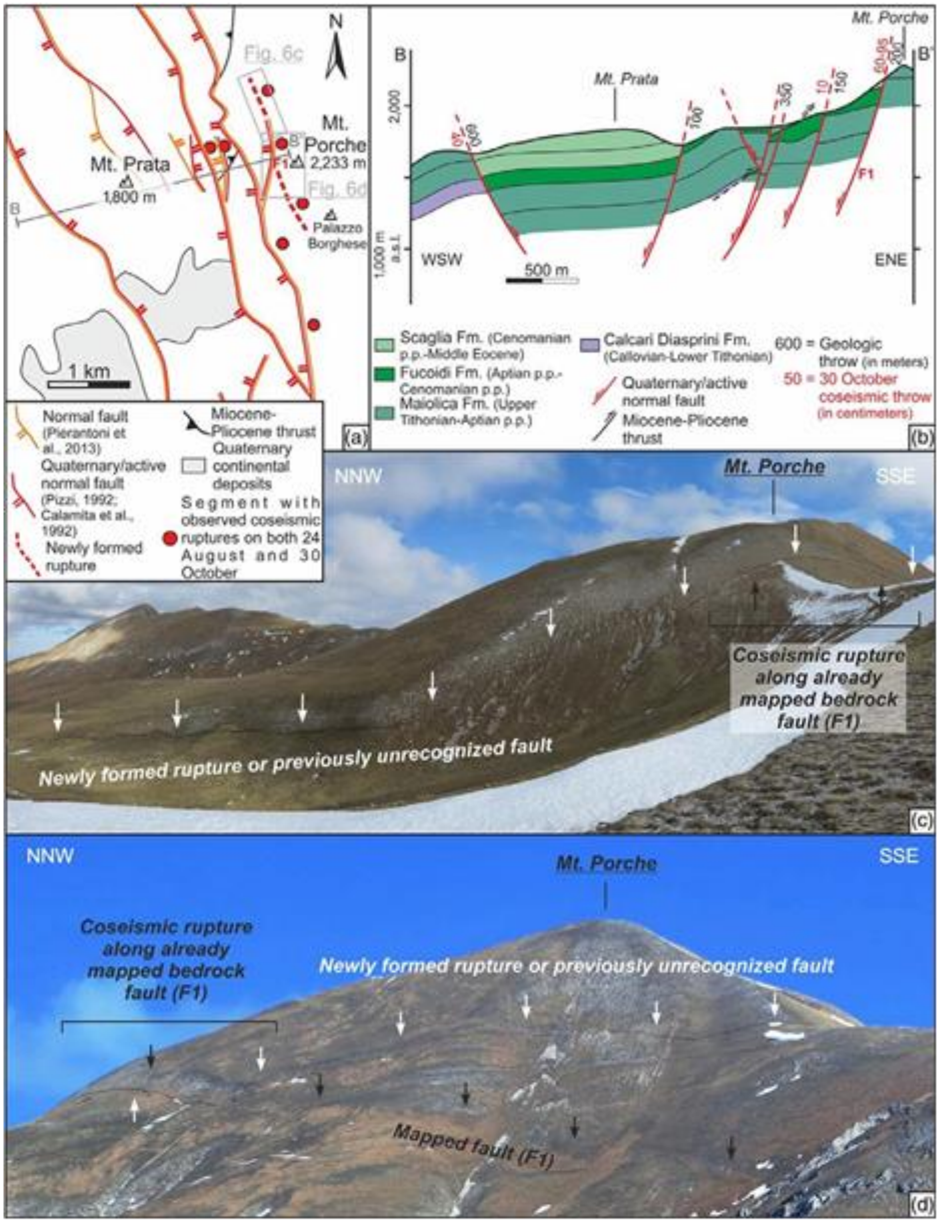
N
Fig. 6c
Mt. Porche
2,233 m
Mt. Prata
1,800 m
F1
Fig. 6d
Palazzo Borghese
B
B'
1 km
(a)
Normal fault (Pierantoni et al., 2013)
Quaternary/active normal fault (Pizzi, 1992; Calamita et al., 1992)
Newly formed rupture
Miocene-Pliocene thrust
Quaternary continental deposits
Segment with observed coseismic ruptures on both 24 August and 30 October
Mt. Porche
Mt. Prata
2,000
1,000 m a.s.l.
WSW
ENE
500 m
F1
Scaglia Fm. (Cenomanian p.p.-Middle Eocene)
Fucoidi Fm. (Aptian p.p.-Cenomanian p.p.)
Maiolica Fm. (Upper Tithonian-Aptian p.p.)
Calcari Diasprini Fm. (Callovian-Lower Tithonian)
600 = Geologic throw (in meters)
50 = 30 October coseismic throw (in centimeters)
Quaternary/active normal fault
Miocene-Pliocene thrust
(b)
NNW
Mt. Porche
SSE
Coseismic rupture along already mapped bedrock fault (F1)
Newly formed rupture or previously unrecognized fault
(c)
NNW
Mt. Porche
SSE
Coseismic rupture along already mapped bedrock fault (F1)
Newly formed rupture or previously unrecognized fault
Mapped fault (F1)
(d)

Figure 6.

Figure 7.

Figure 8.

Figure 9.

Figure 10.

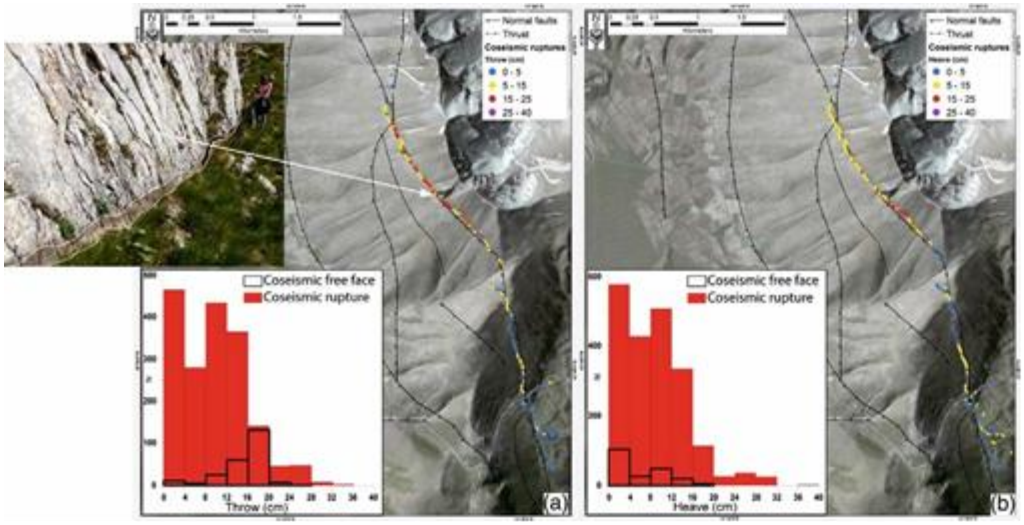

Figure 11.

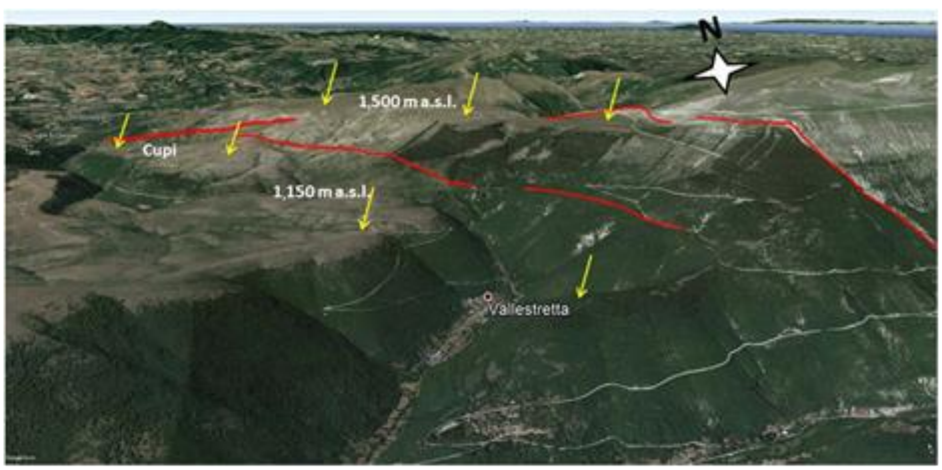

Figure 12.

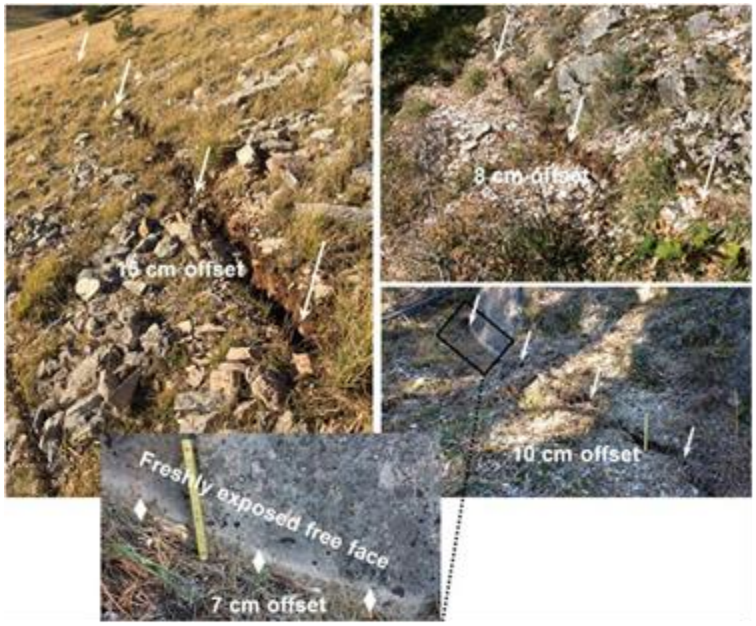

Figure 13.

Figure 14.

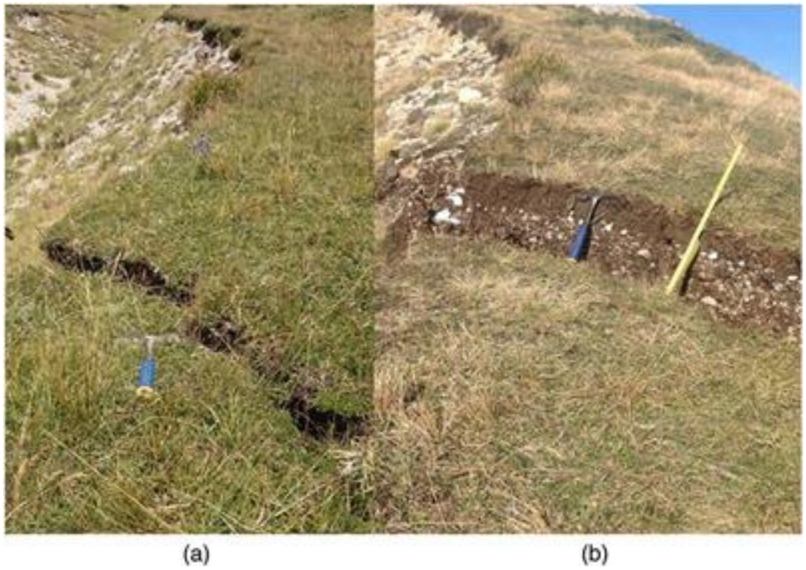

Figure 15.

Figure 16.

Figure 17.

Figure 18.

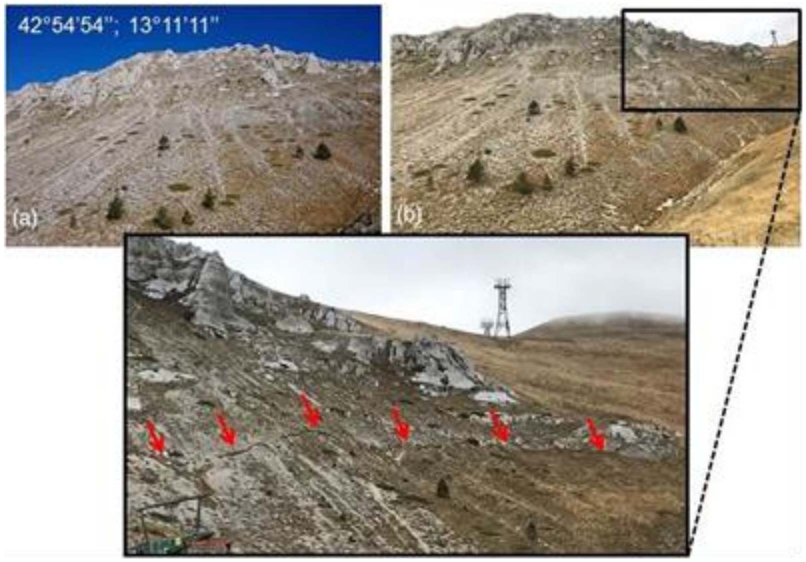

Figure 19.

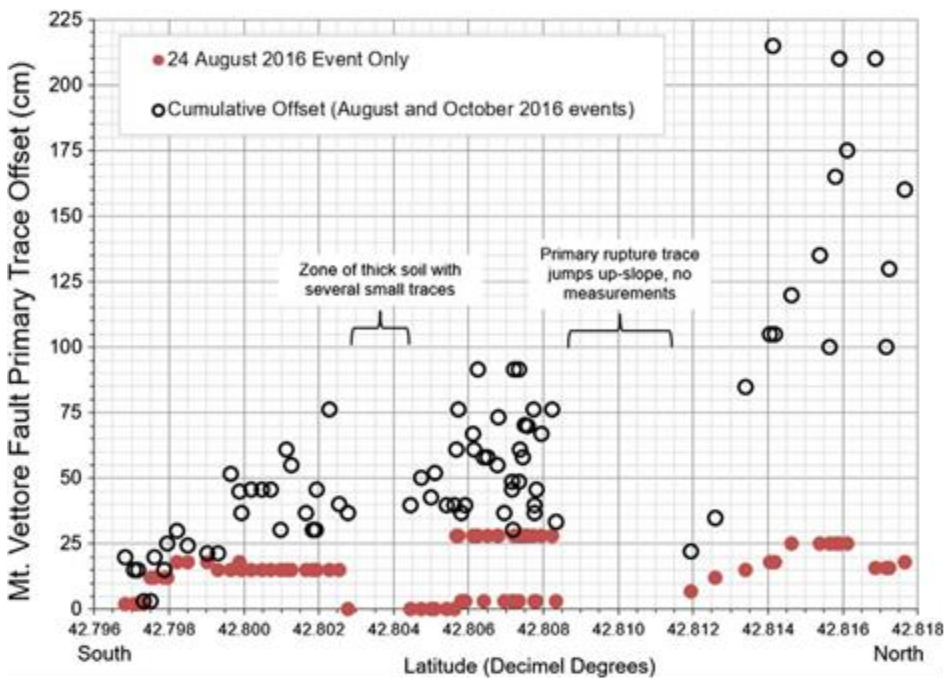

Figure 20.

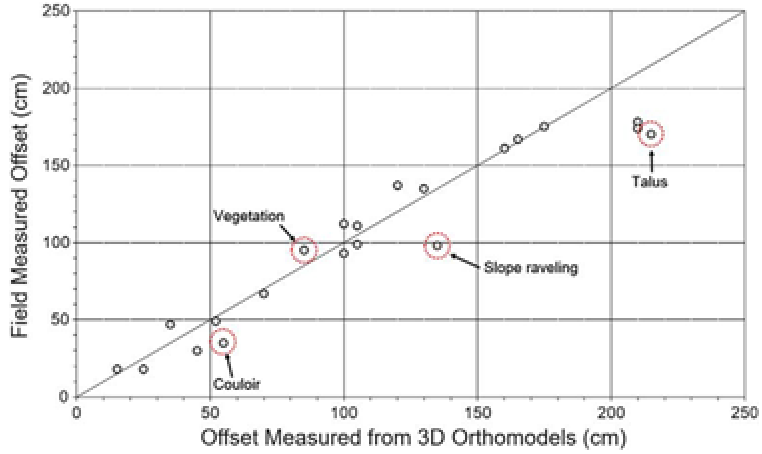

Figure 21.

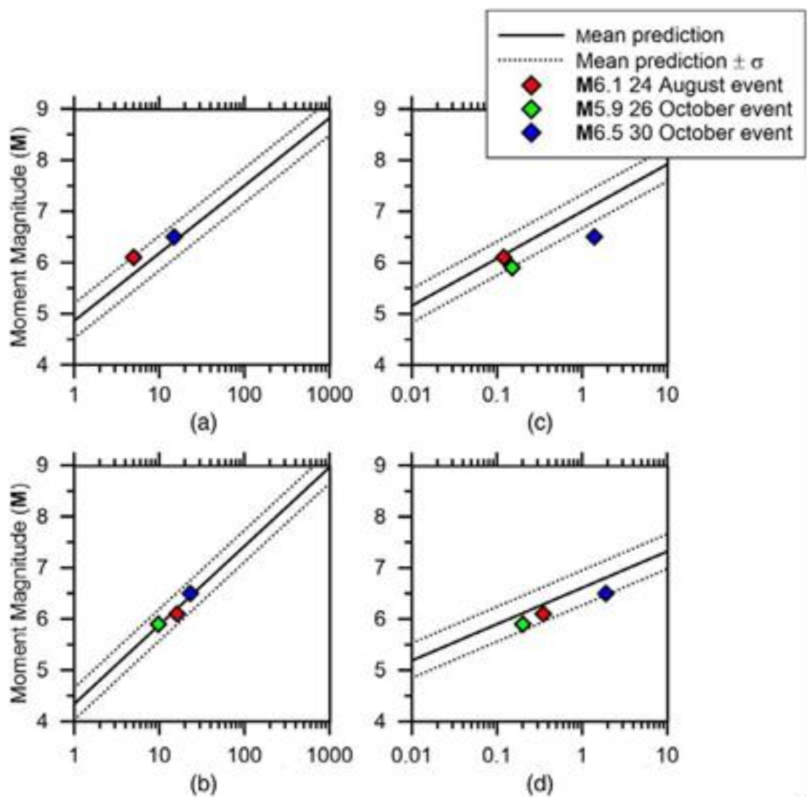

Figure 22.

APPENDIX

This Appendix includes multi-epoch photos taken following the M6.1 24 August and the M6.5 30 October earthquake events. It also includes photos showing areas of the fault that have experienced additional slip (up to ~15% of coseismic throw) over an approximately one-year period following the reconnaissance in November 2016 (related to the 30 October event).

Figure A1. (a) Comparative fault offset, between the 24 August event; and (b) the 30 October event.

Figure A2. (a) Comparative fault offset, between the 24 August event; and (b) the 30 October event.

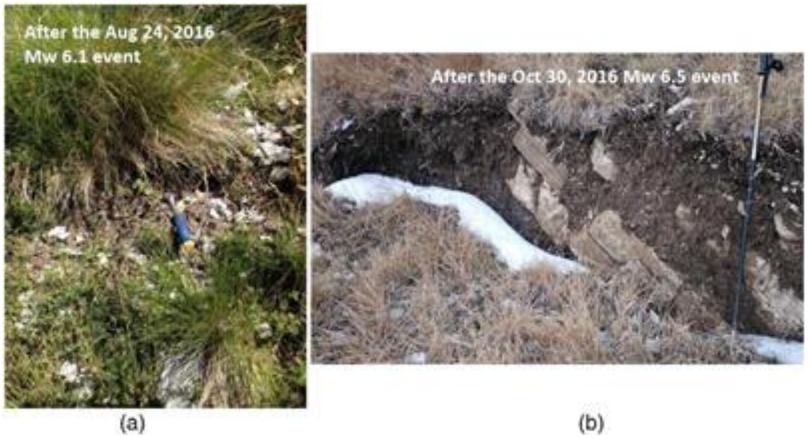

Figure A3. (a) Comparative fault offset, between the 24 August event; and (b) the 30 October event.

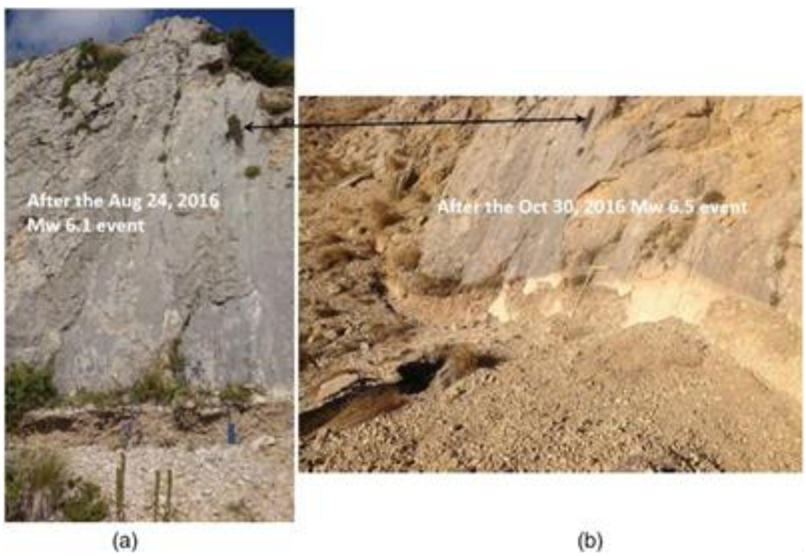

Figure A4. (a) Comparative fault offset, between the 24 August event; and (b) the 30 October event.

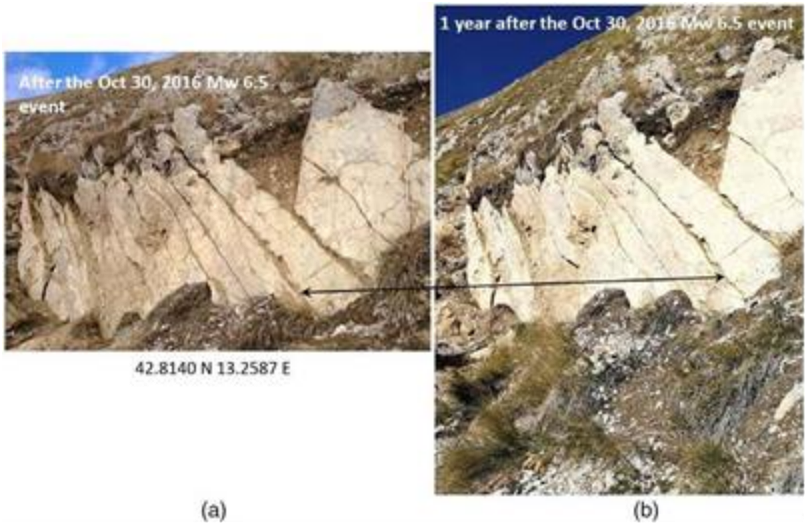

Figure A5. (a) Comparative fault offset, between the 30 October event; and (b) additional slip occurred over an approximately one-year period following the reconnaissance in November 2016.

Figure A6. (a) Comparative fault offset, between the 30 October event; and (b) additional slip occurred over an approximately one-year period following the reconnaissance in November 2016.